Involucrin Modulates Vitamin D Receptor Activity in the Epidermis

Alina D. Schmidt[1,2,3], Charlene Miciano[1,2,3], Qi Zheng[4], Mary Elizabeth Mathyer[1,2,3], Elizabeth A. Grice[4] and Cristina de Guzman Strong[1,2,3,5,6,7]

JID Open

Terminally differentiated keratinocytes are critical for epidermal function and are surrounded by involucrin (IVL). Increased *IVL* expression is associated with a near-selective sweep in European populations compared with those in Africa. This positive selection for increased *IVL* in the epidermis identifies human adaptation outside of Africa. The functional significance is unclear. We hypothesize that IVL modulates the environmentally sensitive vitamin D receptor (VDR) in the epidermis. We investigated VDR activity in $Ivl^{-/-}$ and wild-type mice using vitamin D agonist (MC903) treatment and comprehensively determined the inflammatory response using single-cell RNA sequencing and associated skin microbiome changes using 16S bacterial phylotyping. VDR activity and target gene expression were reduced in $Ivl^{-/-}$ mouse skin, with decreased MC903-mediated skin inflammation and significant reductions in CD4+ T cells, basophils, macrophages, monocytes, and type II basal keratinocytes and an increase in suprabasal keratinocytes. Coinciding with the dampened MC903-mediated inflammation, the skin microbiota of $Ivl^{-/-}$ mice was more stable than that of the wild-type mice, which exhibited an MC903-responsive increase in Bacteroidetes and a decrease in Firmicutes. Together, our studies in $Ivl^{-/-}$ mice identify a functional role for IVL to positively impact VDR activity and suggest an emerging IVL/VDR paradigm for adaptation in the human epidermis.

INTRODUCTION

The epidermis is the outermost tissue of the skin, providing a crucial barrier function against the external environment (Matsui and Amagai, 2015; Watt, 2014). It is composed of a hierarchical structure of proliferating and differentiated epidermal cells or keratinocytes (KCs) that form the essential brick units of the skin barrier. The epidermis is also the primary site of vitamin D3 production (Bikle and Christakos, 2020). KCs are also known to elicit proper recruitment of immune cells in response to breaks in the skin barrier, a key defense mechanism to maintain skin homeostasis (Niec et al., 2021). KCs also respond to microbiota exposure with the induction of key epidermal differentiation gene expression (Meisel et al., 2018; Uberoi et al., 2021). Indeed, the biology of epidermal KCs is complex and challenging, coupled with the need for these cells to quickly adapt amidst differing environments to ensure survival.

Differentiated KCs express many genes encoded within the Epidermal Differentiation Complex locus, which are critical for barrier function (de Guzman Strong et al., 2010; Mischke et al., 1996; Volz et al., 1993; Zhao and Elder, 1997). One important Epidermal Differentiation Complex locus gene is involucrin (*IVL*), whose expression is a major marker for early epidermal differentiation (Rice and Green, 1979). IVL is a scaffold for many cross-linked proteins that together form the mature cornified envelope surrounding the terminally differentiated KC (Eckert and Green, 1986; Kajava, 2000; Nemes et al., 1999; Robinson et al., 1996; Steinert and Marekov, 1995). Given the importance of cornified envelope formation for barrier function, it was surprising to find that $Ivl^{-/-}$ mice exhibit no defects in the epidermal barrier or cornified envelope formation (Djian et al., 2000). However, triple knockout mice for *Ivl*, envoplakin, and periplakin cornified envelope genes exhibited a delay in developmental barrier formation; dry, flaky skin; and persistent hyperkeratosis (Sevilla et al., 2007). Together, these studies revealed that IVL alone is dispensable for skin barrier development but with coinciding envoplakin and periplakin deficiencies, it is critical for epidermal barrier function.

We recently discovered positive selection for a human *IVL* allele in populations of European ancestry (Mathyer et al., 2021). We identified a specific *IVL* haplotype that underwent a near-selective sweep (>95% allele frequency) in contrast to that in Africa (32% allele frequency). The European *IVL* haplotype consists of expression quantitative trait loci associated with increased *IVL* gene expression in the skin

[1]Division of Dermatology, John T. Milliken Department of Medicine, Washington University in St. Louis School of Medicine, St. Louis, Missouri, USA; [2]Center for Pharmacogenomics, John T. Milliken Department of Medicine, Washington University in St. Louis School of Medicine, St. Louis, Missouri, USA; [3]Center for the Study of Itch & Sensory Disorders, Washington University in St. Louis School of Medicine, St. Louis, Missouri, USA; [4]Department of Dermatology, Perelman School of Medicine, University of Pennsylvania, Philadelphia, Pennsylvania, USA; [5]Center for Cutaneous Biology and Immunology Research, Department of Dermatology, Henry Ford Health, Detroit, Michigan, USA; [6]Immunology Program, Henry Ford Cancer Institute, Henry Ford Health, Detroit, Michigan, USA; and [7]Department of Medicine, College of Human Medicine, Michigan State University, East Lansing, Michigan, USA

Correspondence: Cristina de Guzman Strong, Center for Cutaneous Biology and Immunology Research, Department of Dermatology, Immunology Program, Henry Ford Cancer Institute, Henry Ford Health, 1 Ford Place Room 4D46, Detroit, Michigan 48202, USA E-mail: cstrong@hfhs.org

in contrast to relatively lower *IVL* expression in the skin of those of African ancestry. To our knowledge, this study reports a previously unreported recent evolutionary adaptation in the human epidermis. Our finding suggests a selective benefit for increased *IVL* as humans migrated out of Africa. In this study, we revisit the role of IVL for adaptation in the epidermis in response to the environment.

It was recently determined that the vitamin D receptor (VDR) exhibits environmental sensitivity (Romney et al., 2018). This was discovered in killifish, which exhibited differential downstream VDR signaling when grown under different temperature conditions. Motivated by this novel discovery of VDR as an environmentally sensitive receptor and its known expression in epidermal KCs (Stumpf et al., 1979), we reasoned VDR as a potential molecule that could link the levels of IVL in the skin to environmental sensitivity and hence relevant to human epidermal adaptation. VDR is known to stimulate epidermal differentiation when activated by the vitamin D metabolite 1,25-dihydroxyvitamin D produced by KCs (Bikle, 2011; Hosomi et al., 1983). Knockout mouse studies confirmed a requirement for VDR for epidermal differentiation because VDR null mice exhibited reduced levels of IVL, FLG, and loricrin (Bikle et al., 2006; Xie et al., 2002), resulting in a defective permeability barrier (Oda et al., 2009) and immune response (Muehleisen et al., 2012; Schauber et al., 2007). Interestingly, VDR and vitamin D3 levels decrease upon IVL-marked terminal differentiation, suggesting IVL-associated negative feedback regulation for VDR (Horiuchi et al., 1985; Pillai et al., 1988). Moreover, VDR nuclear localization was found to be significantly reduced in the epidermis of the normal skin of black donors compared to that of white donors (Hahn and Supp, 2017) whose genotypes we have determined to be more commonly associated with relatively increased *IVL* (Mathyer et al., 2021). The findings using knockout mice and in vitro studies highlight a putative relationship between IVL and VDR. The more recent study using diverse human skin further suggests a role for higher IVL levels and its potential direct, downstream dosage effect on VDR to modulate epidermal function and underlie population-specific human skin adaptation.

We hypothesized a role for IVL to modulate VDR activity as a mode by which the epidermis adapts to the environment. To test this hypothesis, we investigated the VDR function in the epidermis of *Ivl*⁻/⁻ mice with vitamin D agonist (MC903; Tocris, Minneapolis, MN) exposure and determined the impact using single-cell RNA sequencing (scRNA-seq), flow cytometry, and 16S ribosomal RNA bacterial phylotyping to assess VDR-activated skin inflammation and the anticipated associated changes to the skin microbiome. In this study, we report decreased VDR activity and Vitamin D−responsive gene expressions in *Ivl*⁻/⁻ mice that exhibited reduced MC903-induced inflammation marked by scRNA-seq identification for decreased basophils, macrophages, monocytes, and CD4⁺ T cells and subsequent validation for decreased CD11b⁺ IgE⁺ basophils and CD4+ T cells and newly discovered increase in CD11b⁺ IgE^high mast cells by flow cytometry. The decrease in VDR-mediated inflammation in *Ivl*⁻/⁻ mice coincided with no phylum level changes to the skin microbiome in contrast to that in the wild type (WT) that

exhibited an MC903-responsive dysbiosis with an increase in Bacteroidetes and a decrease in Firmicutes. Together, our findings identify a functional role for IVL to positively impact VDR activity for the skin immune response in the epidermis.

RESULTS

VDR-mediated inflammation is reduced in MC903-treated *Ivl*⁻/⁻ mouse skin

We investigated VDR function in *Ivl*⁻/⁻ and WT mice by way of MC903-mediated activation. *Ivl*⁻/⁻ and WT mouse ear skin was treated daily for 12 days with MC903, which resulted in skin inflammation (Kim et al., 2013; Li et al., 2006; Moosbrugger-Martinz et al., 2017; Walsh et al., 2019). MC903-treated WT mice exhibited ear thickening and scaling compared with ethanol-treated mice (Figure 1a). By contrast, MC903-treated *Ivl*⁻/⁻ mice exhibited less ear thickening and scaling. Histological findings further identified epidermal hyperplasia and hyperkeratosis observed in MC903-treated WT ear skin that was strikingly less evident in MC903-treated *Ivl*⁻/⁻ and absent in ethanol-treated ear skin (Figure 1b). We assessed the longitudinal development of ear thickness over the 12-day treatment period and found an overall trend for decreased
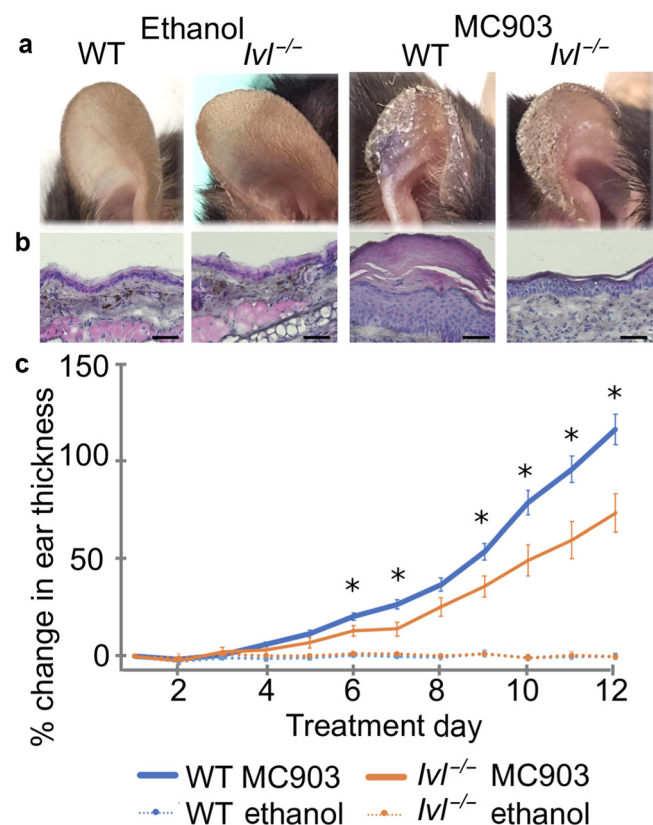
Figure 1. Reduced VDR-mediated inflammation in MC903-treated *Ivl*⁻/⁻ mouse skin. (a) MC903-treated *Ivl*⁻/⁻ mouse ears displayed less scaling and thickness than WT skin. (b) H&E histology staining revealed epidermal hyperkeratosis and hyperplasia in WT ear skin versus in *Ivl*⁻/⁻. Bar = 50 μm. (c) Percentage change in ear thickness (inflammation) was significantly reduced in MC903-treated *Ivl*⁻/⁻ (n = 10, orange) versus in WT mice (n = 15, blue) on days 6 and 7 and days 9−12 versus on day 0. *P < 0.05; one-way ANOVA with posthoc Tukey HSD. Data are presented as error bars ± SEM. No percentage change was observed in ethanol-treated control ears (*Ivl*⁻/⁻, n = 10, dotted orange; WT, n = 15, dotted blue). HSD, honestly significant difference; IVL, involucrin; VDR, vitamin D receptor; WT, wild-type.

MC903-induced skin inflammation in $Ivl^{-/-}$ mice compared with that in WT mice (Figure 1c and Supplementary Figure S1). Decreased inflammation in $Ivl^{-/-}$ mice was significant on days 6 and 7 and for each of days 9−12 (day 6, $P = 0.044$; day 7, $P = 0.016$; day 9, $P = 0.039$; day 10, $P = 0.016$; day 11, $P = 0.007$; and day 12, $P = 0.004$) (one-way ANOVA with posthoc Tukey honestly significant difference). Together, our findings for decreased skin inflammation in MC903-treated $Ivl^{-/-}$ adult mice identify decreased VDR activity in $Ivl^{-/-}$ epidermis.

scRNA-seq identifies a decrease in vitamin D−responsive gene expressions and decreased basophils, CD4+ T cells, macrophages, monocytes, and basal II KCs and increased suprabasal KCs in MC903-treated $Ivl^{-/-}$ skin
We next determined the cell types that underlie the VDR-mediated inflammatory response at a single-cell resolution using scRNA-seq. Single-cell suspensions from MC903-treated ear skin from $Ivl^{-/-}$ and WT mice were obtained for scRNA-seq (10X Genomics, Pleasanton, CA). A total of 25,799 single cells were sequenced and analyzed from both $Ivl^{-/-}$ and WT mice (n = 2 for each genotype). Seurat4.0 clustering analyses (Hao et al., 2021) identified 20 cell populations in MC903-treated ear skin (Figure 2a). KCs comprise a majority of the populations, with 13 distinct KC clusters that were identified in both genotypes (Figure 2b). In addition, five immune cell types were found, including basophils, macrophages, monocytes, NK T cells, and CD4+ T cells, with the remaining two populations comprised of fibroblasts and melanocytes. We confirmed the annotation of the cell clusters using gene markers specific to each cell population (Joost et al., 2016) (Supplementary Tables S1 and S2).

We next investigated the impact of MC903 treatment on vitamin D−responsive gene expression in $Ivl^{-/-}$ mice that exhibited a dampened VDR-mediated inflammatory response. Fourteen VDR-regulated genes in gene set enrichment analysis (GOBP_RESPONSE_TO_VITAMIN_D; MM6812) were expressed in at least one scRNA-seq cell cluster for either MC903-treated $Ivl^{-/-}$ or WT skin (Figure 2c and Supplementary Figure S2). Of these, 10 genes were differentially expressed in at least one scRNA-seq cell cluster in MC903-treated $Ivl^{-/-}$ skin versus that in WT skin (adjusted $P < 0.05$) (Supplementary Table S3). A majority of these gene expression differences in $Ivl^{-/-}$ skin were decreased (38 of 41 clusters) and were found primarily in the KC clusters (17 of 38 decreased clusters). *Vdr*, *Cyp24a1*, *Snw1*, *Pdia3*, and *Rxra* were the top five differentially expressed genes that were observed in at least three clusters (Figure 2c). *Vdr*, *Snw1*, and *Pdia3* were all decreased in basal cycling (0), suprabasal cycling (3), and suprabasal infundibular (6) KCs in MC903-treated $Ivl^{-/-}$ mice. More importantly, *Vdr* was the top gene that was found to have the greatest number of KC clusters exhibiting differential expression, a total of nine that were all decreased in $Ivl^{-/-}$ mice. By contrast, VDR-regulated *Cyp24a1* was increased in several $Ivl^{-/-}$ KC clusters and melanocytes. *Cyp24a1* encodes 24-hydroxylase that breaks down active vitamin D (Makin et al., 1989; Reddy and Tserng, 1989; Schlingmann et al., 2011). The finding for increased *Cyp24a1* in MC903-treated $Ivl^{-/-}$ skin suggests a compensatory mechanism in response to MC903 and likely non-VDR regulated,

given the decreased *Vdr* expression in these mice. Together, our findings identify significant decreases in VDR and vitamin D−responsive genes that underlie the dampened MC903-mediated inflammation in $Ivl^{-/-}$ mice.

We further determined whether there was a difference in the proportions between each scRNA-seq population in MC903-treated $Ivl^{-/-}$ mice compared with that in WT mice. The proportions for each of the five cell populations were significantly reduced in MC903-treated $Ivl^{-/-}$ mice: basophils, macrophages, basal IIb KCs, CD4+ T cells, and monocytes (Figure 2d) (chi-square goodness of fit $P < 0.00001$, $P < 0.00001$, $P < 0.00001$, $P < 0.0455$, and $P < 0.00014$, respectively). However, suprabasal KCs were significantly increased in MC903-treated $Ivl^{-/-}$ ear skin (Figure 2d) (chi-square goodness of fit $P < 0.028$) and concomitant with a decrease in basal IIb KCs. The finding suggests a higher turnover in basal IIb KCs and a downstream effect for the increased number of suprabasal KCs. The reduction in basophils led us to further investigate the significance of IL-4 and IL-6, which are also known key drivers for MC903-induced skin inflammation (Hussain et al., 2018; Kim et al., 2014; Walsh et al., 2019). Our scRNA-seq analysis resolved predominant IL-4 and IL-6 expressions in basophils as shown in MC903-treated mice and for which basophil numbers were significantly decreased in the $Ivl^{-/-}$ mice (Figure 2d and e). In summary, scRNA-seq resolves the single-cell architecture of the dampened MC903-induced inflammation in $Ivl^{-/-}$ mice identifying reduced basophils, macrophages, CD4+ T cells, and monocytes and a notable KC response (basal IIb KC depletion with increased suprabasal cells) and further highlights skin immune cellular interconnectivity.

Flow cytometry validates decreased CD4+ T cells and basophils and reveals increased mast cells in MC903-treated $Ivl^{-/-}$ mouse skin
We sought to validate the scRNA-seq−identified immune cell types that were reduced in MC903-treated $Ivl^{-/-}$ mice compared with those in WT mice by flow cytometry. CD4+ T cells, CD11c+ dermal dendritic cells, granulocytes, monocytes, eosinophils, and CD8+ T cells were previously determined to be increased on the basis of immunofluorescent and histological findings in MC903-induced inflamed skin (Li et al., 2006). However, of the CD45+ leukocytes in the MC903-treated skin, we found no significant differences in dendritic cells (CD11c+), eosinophils (CD11b+, Ly6g−), neutrophils (CD11b+, Ly6g+), and B cells (CD19+) between $Ivl^{-/-}$ and WT mice (Supplementary Figure S3). We also did not find significant differences in monocytes (CD11b+, Ly6g−, F4/80−) and macrophages (CD11b+, Ly6g−, F4/80+) (Figure 3a and b). However, both CD4+ T cells and CD11b+ IgE+ basophils were significantly reduced in $Ivl^{-/-}$ compared with those in WT-treated ear skin (Figure 3a and b) (one-sided t-test, $P < 0.04$ and $P < 0.05$, respectively). Interestingly, we also observed an increase in a distinct population of CD11b+ IgE^high cells in MC903-treated $Ivl^{-/-}$ skin, representative of mast cells that were significantly increased compared with those in MC903-treated WT ear skin (one-sided t-test, $P < 0.03$) (Figure 3a and b). Together, our flow cytometry results confirm our scRNA-seq findings for decreased basophil and CD4+ T-cell infiltrates, with an additional discovery for increased CD11b+ IgE^high mast cells in MC903-treated $Ivl^{-/-}$ mice.
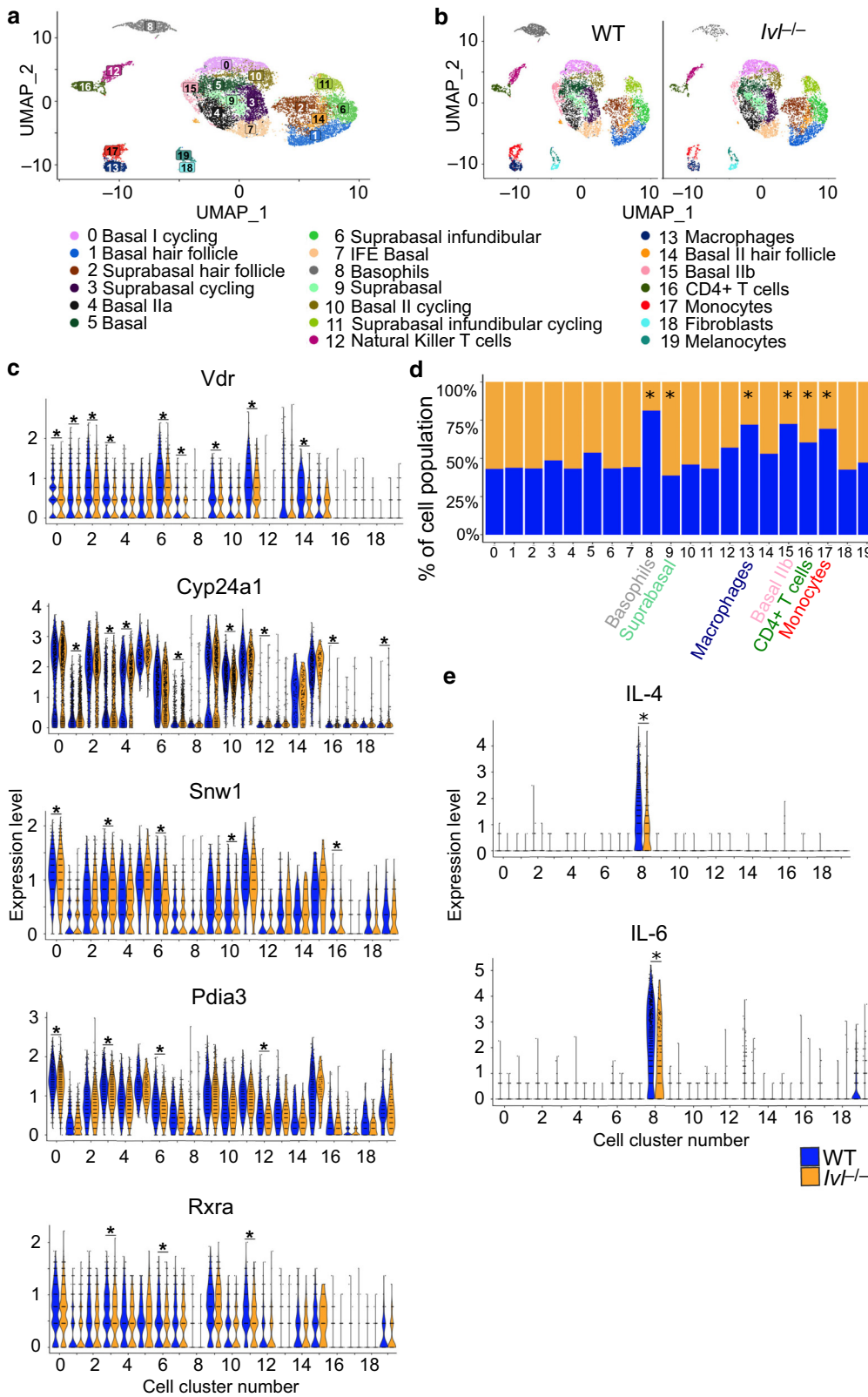
Figure 2. scRNA-seq identifies differential expressions for vitamin D−responsive genes and decreases in basophils, macrophages, CD4+ T cells, monocytes, and basal II keratinocytes and an increase in suprabasal keratinocytes in MC903-treated *Ivl*$^{-/-}$ skin. (**a**) UMAP of scRNA-seq−identified cell types in both MC903-treated WT and *Ivl*$^{-/-}$ skin (n = 2 per genotype). (**b**) Individual UMAPs of cell types in MC903-treated WT (left) and *Ivl*$^{-/-}$ (right) skin. (**c**) Vitamin D−responsive *Vdr, Cyp24a1, Snw1, Pdia3,* and *Rxra* genes are differentially expressed between MC903-treated WT and *Ivl*$^{-/-}$ skin and ranked by the number of clusters with significance and by the number found in keratinocyte clusters (Wilcoxon signed-rank test, *adj. $P < 0.05$, also see Supplementary Table S3). (**d**) Bar plots (proportions of cells) for WT (blue) and *Ivl*$^{-/-}$ (orange). Basophils, macrophages, CD4+ T cells, monocytes, and basal IIb keratinocytes were decreased. Suprabasal keratinocytes were increased in *Ivl*$^{-/-}$ versus in WT (chi-square goodness of fit *$P < 0.05$). (**e**) Predominant IL-4 and IL-6 expressions in basophils, which were reduced in MC903-treated *Ivl*$^{-/-}$ versus WT skin. adj., adjusted; IVL, involucrin; scRNA-seq, single-cell RNA sequencing; UMAP, Uniform Manifold Approximation and Projection; WT, wild-type.
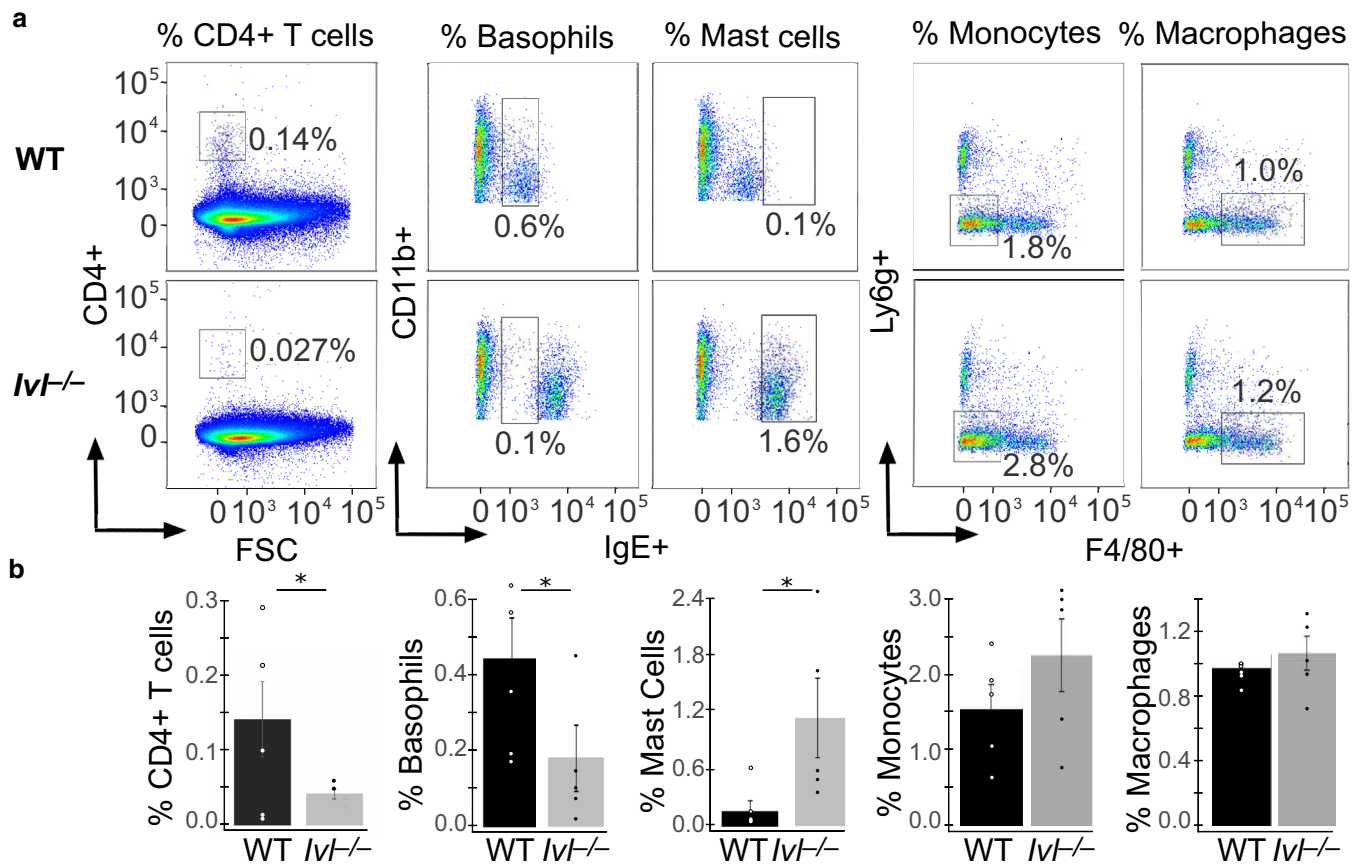
Figure 3. CD4$^+$ T cells and CD11b$^+$ IgE$^+$ basophils are reduced and CD11b$^+$ IgE^{high} mast cells are increased in MC903-treated *Ivl*$^{-/-}$ mouse skin. (**a**) Flow cytometry pseudo-color dot plots for CD45$^+$-gated cell types shown in representative MC903-treated WT and *Ivl*$^{-/-}$ ear skin (day 12). (**b**) Bar graphs of cell-type mean percentages are also shown. CD4$^+$ T cells and CD11b$^+$ IgE$^+$ basophils in MC903-treated *Ivl*$^{-/-}$ ear skin were significantly decreased. CD11b$^+$ IgE^{high} mast cells were also significantly increased in MC903-treated *Ivl*$^{-/-}$ ear skin. (CD4$^+$ T cells, *$P < 0.04$; basophils, $P < 0.05$; and mast cells, *$P < 0.03$; one-sided *t*-test). No significant differences were found for both monocytes and macrophages (n = 5 per genotype). Data are presented as error bars ± SEM. IVL, involucrin; WT, wild-type.

MC903-treated WT skin exhibit increased Bacteroidetes and decreased Firmicutes, whereas *Ivl*$^{-/-}$ untreated skin exhibit increased Firmicutes (*Streptococcus* and *Aerococcus*) and decreased Bacteroidetes (*Muribaculaceae*) operational taxonomic units

We next examined the impact of VDR-mediated inflammation on *Ivl*$^{-/-}$ and WT skin microbiomes. Specific microbiome changes (dysbiosis) are sufficient to drive skin inflammation as observed in barrier-impaired, ADAM17-deficient mice (Kobayashi et al., 2015). However, whether VDR-mediated inflammation drives microbial changes per se is an underexplored area of investigation. The dampened VDR activity and decreased *Vdr* and vitamin D−responsive gene expression in *Ivl*$^{-/-}$ skin also provide us with the opportunity to more directly address the microbial changes specific to VDR activity that are active in WT and compromised in *Ivl*$^{-/-}$ skin. Because microbiota exposure induces host expression of IVL in the skin (Meisel et al., 2018; Uberoi et al., 2021), we further explored the significance of IVL for shaping microbial community structure.

To profile the skin microbiota dynamics, we used 16S ribosomal RNA sequencing of the V1−V3 hypervariable region to identify bacterial taxa from ear swab collections from mice aged 12 weeks before and after MC903 treatment. The 16S microbiome sequencing reads were individually phylotyped and subsequently clustered into phylogeny-based operational taxonomic units (OTUs) (Zheng et al., 2018). We first assessed the beta (inter-sample) diversity with respect to MC903 treatment in *Ivl*$^{-/-}$ and WT skin and observed that clustering between microbial communities was significantly associated with both genotypes (WT or *Ivl*$^{-/-}$) and MC903 treatment (before or after) (Figure 4a) ($P < 0.005$, permutational ANOVA test) (GreenGenes, version 13.8 [DeSantis et al., 2006]). Closer examination of the microbial phyla on untreated WT skin revealed a composition dominated by the phylum Firmicutes and phylum Bacteroidetes consistent with previous reports in WT murine ear skin microbiota (Moskovicz et al., 2021; Ren et al., 2017) (Figure 4b). By contrast, we found reductions in Bacteroidetes, Actinobacteria, and Verrucomicrobia and an increase in Firmicutes in *Ivl*$^{-/-}$ untreated skin compared with those in WT skin (Figure 4b). We next compared the alpha diversity (intra sample) of untreated WT and *Ivl*$^{-/-}$ skin by calculating the Shannon Index, which takes into account both the richness and evenness of OTUs observed in a sample. We detected a significant depletion in the alpha diversity of untreated *Ivl*$^{-/-}$ skin compared with that in WT skin ($P < 0.001$, *t*-test) (Figure 4c).
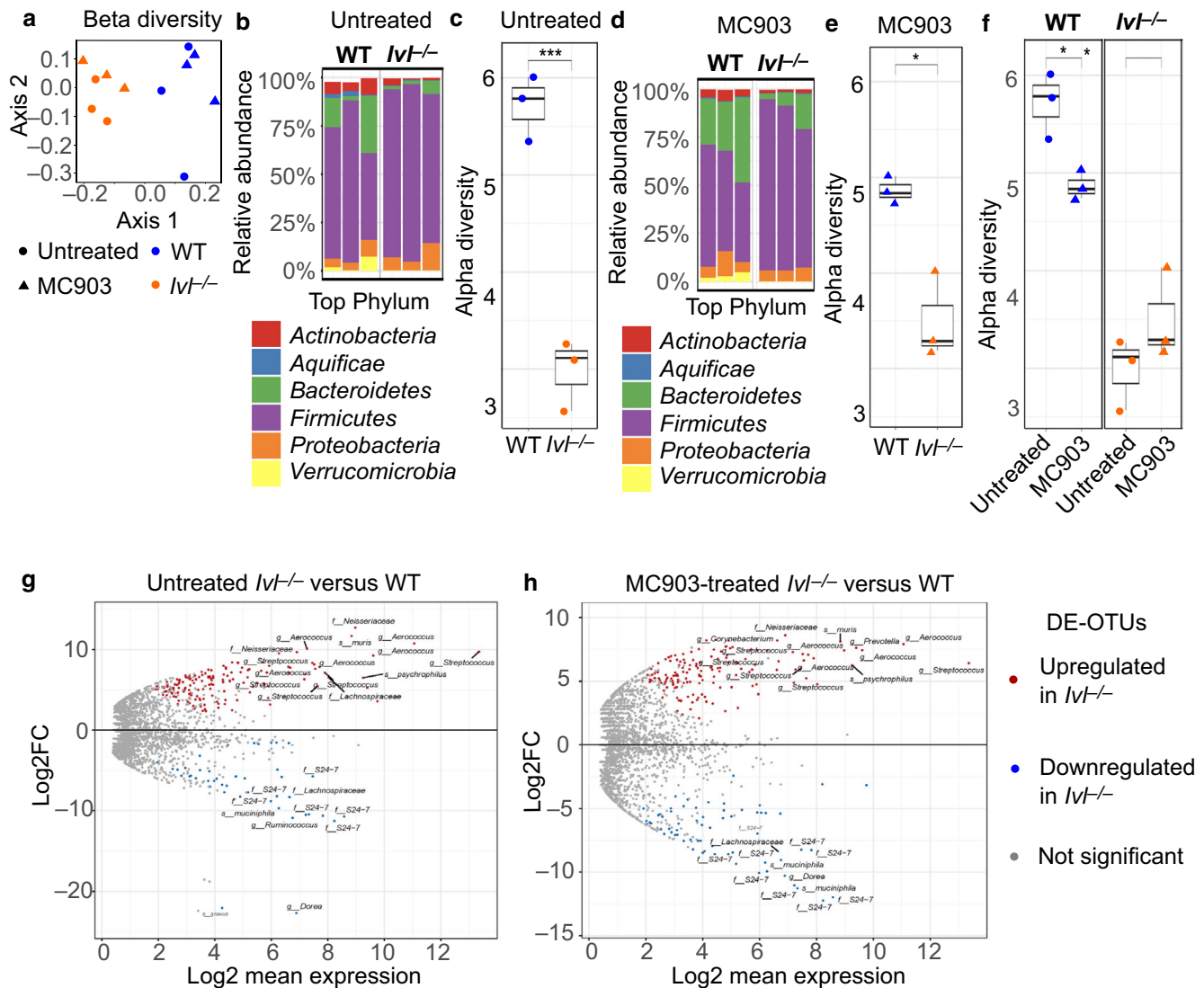
Figure 4. MC903-treated WT skin show increased Bacteroidetes and decreased Firmicutes, whereas *Ivl*^{−/−} untreated skin exhibit increased *Streptococcus* and *Aerococcus* (Bacteroidetes) taxa. (**a**) Clustering between microbial communities based on unweighted UniFrac distance (beta diversity) was significantly associated with both genotype (WT or *Ivl*^{−/−}) and MC903 treatment (before or after). Axis 1 (26.1% variance) and axis 2 (16.3% variance) (OTU_dist ∼ study_group * TimePoint, $P < 0.005$). (**b**) Relative abundance of top phylum-level OTUs in untreated WT and *Ivl*^{−/−} skin (WT and *Ivl*^{−/−}, each n = 3). (**c**) Decreased alpha diversity (Shannon index) in untreated *Ivl*^{−/−} versus WT skin (***$P < 0.01$). (**d**) Relative abundance of top phylum-level OTUs in MC903-treated WT and *Ivl*^{−/−} skin. (**e**) Decreased alpha diversity in MC903-treated *Ivl*^{−/−} versus WT skin (*$P < 0.05$). (**f**) Alpha diversity is significantly reduced in MC903-treated WT skin (*$P < 0.05$) but not in MC903-treated *Ivl*^{−/−} skin. DE-OTU MA plots of (**g**) untreated *Ivl*^{−/−} versus WT skin; *Streptococcus*, *Aerococcus*, *Lachnospiraceae*, and *Muris* (phylum Firmicutes) comprise a majority of the top 15 significantly upregulated DE-OTUs, and *Muribaculaceae* (phylum Bacteroidetes) represent the most common top 15 significantly downregulated DE-OTUs and (**h**) MC903-treated *Ivl*^{−/−} versus WT skin. *Streptococcus* and *Aerococcus* are also found in a majority of the top 15 significantly upregulated DE-OTUs, with *Muribaculaceae* in a majority of the top 15 significantly downregulated DE-OTUs. All MA plots are shown with FDR < 0.1 and log$_2$FC ≥ 1. DE-OTU, differentially expressed operational taxonomic unit; FC, fold change; FDR, false discovery rate; IVL, involucrin; OTU, operational taxonomic unit; WT, wild type.

We next determined the longitudinal effect of MC903 treatment on the skin microbiota. MC903 treatment in WT skin resulted in an increase in phylum Bacteroidetes and a decrease in phylum Firmicutes compared with untreated skin (Figure 4d). In contrast, MC903 treatment in *Ivl*^{−/−} skin did not change the phylum composition of the skin microbiota compared with that in the untreated *Ivl*^{−/−} skin (Figure 4d). However, alpha diversity in MC903-treated *Ivl*^{−/−} skin was significantly reduced compared with that in MC903-treated WT skin and correlates with the dampened skin inflammation in *Ivl*^{−/−} treated skin compared with that in WT-treated

skin ($P < 0.05$) (Figure 4e). Relative to that in untreated skin, alpha diversity in WT skin was significantly reduced after MC903 treatment (Figure 4f) ($P < 0.05$, t-test). In contrast, alpha diversity in *Ivl*^{−/−} mice did not change after MC903 treatment, albeit with a slight increase compared with that of baseline skin (Figure 4f). Together, our results reveal potential dysbiosis in *Ivl*^{−/−} baseline skin marked by a decrease in Bacteroidetes, Actinobacteria, and Verrucomicrobia and an increase in Firmicutes phyla. These changes were also consistent with a significant decrease in alpha diversity that persisted even upon MC903 treatment. We further

identified dysbiosis in our longitudinal study of WT skin upon MC903 treatment marked by an increase in Bacteroidetes, a decrease in Firmicutes, and a significant reduction in alpha diversity.

We next determined the differentially enriched OTUs (DE-OTUs) that underlie the microbiota differences observed in $Ivl^{-/-}$ skin and upon MC903 treatment in WT skin. We compared the abundance of each phylogeny-based OTU per mouse group before and after treatment (Love et al., 2014). In untreated skin, we identified 122 upregulated and 28 downregulated DE-OTUs in $Ivl^{-/-}$ skin compared with those in WT skin (Figure 4g and Supplementary Table S4). A majority of the top 15 upregulated OTUs in $Ivl^{-/-}$ untreated skin (66%) were comprised of phylum Firmicutes (*Aerococcus, Streptococcus, Lachnospiraceae,* and *Muris*). By contrast, the most common taxa of the top 15 downregulated OTUs in $Ivl^{-/-}$ untreated skin were *Muribaculaceae* (Bacteroidetes phylum) (47%), formerly known as S24-7 (Ormerod et al., 2016). In MC903-treated skin, we identified a total of 115 upregulated and 52 downregulated DE-OTUs (Figure 4h and Supplementary Table S5) in $Ivl^{-/-}$ skin versus those in WT skin. Similar to untreated skin, a majority (66%) of the top 15 upregulated OTUs in MC903-treated $Ivl^{-/-}$ skin were comprised of members from the phylum Firmicutes (*Aerococcus* and *Streptococcus*). Again, similar to untreated skin, a majority (60%) of the downregulated OTUs were Bacteroidetes (*Muribaculaceae*).

In summary, our results suggest changes to the skin microbiota in $Ivl^{-/-}$ skin that were stable even after MC903 treatment. Our longitudinal study further identifies alterations to the microbiota in WT and not in $Ivl^{-/-}$ skin with decreased VDR-mediated inflammation. This supports the hypothesis that VDR-mediated inflammation can drive dysbiosis. Because housing conditions can influence the skin microbiota, future studies using isolated cages and additional single-housed mice can further bolster these findings and provide insight into the cause-and-effect relationship between host and microbiota.

DISCUSSION

Our study identifies a functional role for *IVL* to positively regulate VDR activity in the epidermis. In this study, we find that VDR activation and several vitamin D−responsive genes, including *Vdr*, are reduced in MC903-treated $Ivl^{-/-}$ mice, resulting in a dampened VDR-mediated inflammatory response. The response is characterized by a significant reduction in CD4+ T cells; decreases in basophils, monocytes, macrophages, and basal II KCs; and a concomitant increase in suprabasal KCs. Indeed, MC903 is an analog of the natural VDR ligand, 1,25-dihydroxyvitamin D; however, its topical application also stimulates VDR activity, resulting in skin inflammation, albeit at a lower calcemic activity (Carlberg, 2003). We further validated our scRNA-seq findings for increased CD4+ T cells and basophils in MC903-treated WT skin and also discovered an increase in mast cells in MC903-treated $Ivl^{-/-}$ skin. Although flow cytometry did not fully recapitulate the scRNA-seq findings for monocytes and macrophages, not all monocytes and macrophage clusters as determined by scRNA-seq directly correlate with cell surface marker expression (Sanin et al., 2022). Indeed,

recent scRNA-seq studies have determined that multiple subsets of monocytes and their derived macrophages exist and that each is marked by dynamic heterogeneity in its transcriptional programs (Sanin et al., 2022; Villani et al., 2017; Zilionis et al., 2019). This also creates even more challenges to further resolve these subset(s) and ascribe function. Nevertheless, increased monocytes have been reported in several MC903 studies (Kim et al., 2013; Li et al., 2006; Walsh et al., 2019). Future studies are needed to further resolve the monocyte subsets impacted in the context of MC903-mediated inflammation and other inflammatory conditions. In addition, $Ivl^{-/-}$ skin also exhibited microbial dysbiosis with increases in Firmicutes phyla—*Streptococcus* and *Aerococcus*—and a decrease in Bacteroidetes *Muribaculaceae*, which was sustained even after MC903 treatment. Together, our results identify a functional role for IVL to facilitate VDR signaling in the epidermis for skin immune crosstalk and cellular composition as well as for impacting the microbial community structure.

Previous work in vitro suggested potential negative feedback for IVL on VDR (Horiuchi et al., 1985; Pillai et al., 1988). VDR and vitamin D3 levels concomitantly decreased and coincided with the onset of IVL-marked terminal differentiation as determined in cultured KCs. However, our in vivo work in mice challenges this notion and rather establishes that the presence of IVL instead positively regulates epidermal VDR activity. This is further supported by our scRNA-seq findings in $Ivl^{-/-}$ KC clusters for decreased *Vdr* and *Snw1*, *Pdia3*, and *Rxra* that coregulate with VDR (Chen et al., 2013; Quack and Carlberg, 2000; Zhang et al., 2003).

The increase in mast cells observed in MC903-treated $Ivl^{-/-}$ mice is notable despite the dampened skin inflammation yet observed dysbiosis. Mast cells are long lived (up to 30 days) in contrast to short-lived basophils (up to 3 days) and hence are likely to reflect a more sustained cellular response to an environmental trigger (Igawa and Di Nardo, 2017). Interestingly, it was recently discovered that germ-free mice have immature mast cells (Wang et al., 2017). Skin microbiota reconstitution in these mice facilitated normal mast cell maturation, thus identifying a functional role for microbiota in shaping mast cell differentiation. Based on these findings, we speculate that the observed mast cell increase in MC903-treated $Ivl^{-/-}$ mice may likely arise from previous skin dysbiosis and warrants future investigations.

In addition, our findings for potential dysbiosis in *Ivl*-deficient mouse skin suggest a requirement for IVL to maintain microbial homeostasis in comparison with its reference WT isogenic C57Bl/6 mouse strain. We further identify dysbiosis associated with VDR-mediated inflammation in WT skin. Indeed, additional studies are needed to completely exclude the possibility of cage effects in comparing IVL-deficient with WT skin microbiota at baseline; however, we included the collection and analysis of negative- and positive-control specimens to minimize this concern. With our longitudinal study design, we were able to capture the changes in the microbiome due to treatment. Even with the observed microbiota changes, the microbiome of $Ivl^{-/-}$ skin does not appear to give rise to pathogenic infection even after MC903 treatment and also over time because we did not observe any

overt infections in MC903-treated mice or in adult $Ivl^{-/-}$ mice up to age 2 years in pathogen-free housing conditions (data not shown). An additional interpretation is that the presence of IVL may promote a niche-specific microbiome with enrichment for specific members of the Firmicutes, Proteobacteria, and Bacteroidetes phyla at the expense of the Bacteriodetes phylum *Muribaculaceae* and distinct members of the Firmicutes and Verrumocrobia phyla.

Until now, our current understanding of human skin evolution has been illuminated by the discovery of skin pigmentation as an adaptation to the degree of UVB sun exposure (Jablonski and Chaplin, 2010). Our current research expands our understanding of skin evolution with the identification of IVL-mediated adaptation for the epidermis. Our previous work identified a recent positive selection for increased *IVL* in European populations (Mathyer et al., 2021), suggesting a functional role for *IVL* dosage that we addressed in this paper. Indeed, earlier studies have highlighted genetic innovation for *IVL* with the expansion of glutamine-rich tandem repeats across mammalian and primate clades and the more recent emergence of the late-repeat domain that arose only in humans and continues to expand in repeat numbers across human populations (Djian and Green, 1989; Eckert and Green, 1986; Teumer and Green, 1989; Tseng and Green, 1989). In conclusion, our findings highlight an exciting paradigm for IVL dosage to modulate VDR function that affects epidermal crosstalk and the modulation of the skin immune system.

MATERIALS AND METHODS
Mice
WT and $Ivl^{-/-}$ C57BL/6 mice were group housed in pathogen-free, barrier conditions and approved by the Division of Comparative Medicine Animal Studies Committee (Washington University in St. Louis School of Medicine, St. Louis, MI) and in accordance with the National Institutes of Health Guide for the Care and Use of Laboratory Animals. MC903 treatment (1 nmol) was administered daily to the same ear (ethanol control on the opposite ear) in mice aged 11–14 weeks for 12 days. Ear thickness was measured daily with a Peacock dial thickness gauge caliper (Ozaki MFG, Itabashi, Japan).

Flow cytometry
MC903-treated ear tissue was dissociated (0.25% Trypsin/EDTA; Gibco, Grand Island, NY) at 37 °C (750 r.p.m.) for 90 minutes, and the Fc receptor (eBioscience, Carlsbad, CA) was blocked. Antibodies are listed in Supplementary Materials and Methods. Gates were based on the specificity of cell surface marker versus isotype control staining with dead cell exclusions (Hoechst or 7-aminoactinomycin D positive; Thermo Fisher, Waltham, MA) through BD FACSAria II (BD Biosciences, San Jose, CA) and FlowJo10.6.2 analysis (BD Life Sciences, Ashland, OR).

scRNA-seq
Treated ears were dissociated in trypsin at 37 °C (750 r.p.m.) for 90 minutes and strained before two rounds of centrifugation (300 r.c.f.) for 7 minutes at 4 °C. A total of 20,000 live cells (Hoechst⁻) per sample were captured by flow cytometry (AriaII) and submitted for 10X Genomics library preparation and sequencing. Unfiltered feature-barcode matrix per sample from 10X Cell Ranger was obtained for each $Ivl^{-/-}$ and WT replicate (n = 2 per genotype). Analysis was performed with the R programming environment (version 4.1.0) and Seurat (version 4.0.3) (Hao et al., 2021). Cells were excluded for any of the following criteria: cells of low quality (<700 genes), cell doublets (>8,000 genes), and dead/stressed cells (>60% mitochondrial gene expression). $Ivl^{-/-}$ single cells were downsampled to the WT populations (8,135 cells per genotype). All data were scaled and normalized with the centered-log ratios parameter, followed by principal component analysis (10 principal components), batch correction, and integration using Harmony (Korsunsky et al., 2019). Uniform Manifold Approximation and Projection was determined by FindNeighbors using dimensions 1 through 10 as input parameters and FindClusters with a resolution of 0.8 for cell cluster discovery using the Louvain algorithm. Marker genes were identified separately for each genotyped sample using the FindAllMarkers function. Cell clusters were determined by comparing reference datasets in (Joost et al., 2016) and My Geneset on Immunological Genome Project (immgen.org). Analysis of vitamin D–responsive genes involved the comparisons of gene expression means for genes listed in Gene Set Enrichment Analysis Mouse Gene Set: GOBP_CELLULAR_RESPONSE_TO_VITAMIN_D (MM9698) (Liberzon et al., 2015; Subramanian et al., 2005).

Microbiome
Skin microbiota was collected using premoistened sterile swabs on adult mouse ear skin (cohoused littermates by genotype) before and after 12 days of MC903 treatment (n = 3, WT and $Ivl^{-/-}$ each). Air swabs from each cage were obtained as negative controls. Bacterial swabs were subjected to bacterial genome isolation and submitted for 16S ribosomal RNA microbiome sequencing (V1–V3 regions) on Illumina Miseq (Illumina, San Diego, CA). A total of ∼720,000 reads were obtained with a mean of 30,000 and a median of 29,000 per sample. Quality control was performed with AlignerBoost, version 1.8.3 (Zheng and Grice, 2016), and demultiplexed with Flexbar, version 3.5 (Roehr et al., 2017). Chloroplast and mitochondrial reads that mapped to the taxonomy class Chloroplast or family mitochondria were removed from the analysis. Phylogenetic assignment was obtained using HmmUFOtu, version 1.4.2 (Zheng et al., 2018) with the GreenGene97% OTU database (release 13.8) and pseudo-node on (all OTUs as leaf nodes). Statistics were calculated using the R package phyloseq, version 1.32.0 (McMurdie and Holmes, 2013), and DEseq2, version 1.28.1 (Love et al., 2014). To identify DE-OTUs, 16S microbiome data were converted to DESeq2 objects and ran using a negative binomial linear model as ∼ study_-group*time_point. Thresholds for significant DE-OTUs were false discovery rate < 0.1 and absolute $\log_2$ fold change $\geq$ 1.

ORCIDs
Alina D. Schmidt: http://orcid.org/0000-0001-7317-7868
Charlene Miciano: http://orcid.org/0000-0001-7653-8876
Qi Zheng: http://orcid.org/0000-0002-2582-1222
Mary Elizabeth Mathyer: http://orcid.org/0000-0003-4725-7439
Elizabeth A. Grice: http://orcid.org/0000-0003-3939-2200
Cristina de Guzman Strong: http://orcid.org/0000-0001-8540-9611

AUTHOR CONTRIBUTIONS

Conceptualization: CDGS; Data Curation: ADS, CM, QZ, CDGS; Formal Analysis: ADS, CM, QZ, EAG, CDGS; Funding Acquisition: EAG, CDGS; Investigation: ADS, CM, QZ, MEM, EAG, CDGS; Methodology: ADS, CM, QZ, MEM, EAG, CDGS; Project Administration: EAG, CDGS; Resources: EAG, CDGS; Software: ADS, CM, QZ; Supervision: EAG, CDGS; Validation: ADS, CDGS; Visualization: ADS, CM, QZ, CDGS; Writing − Original Draft Preparation: ADS, MEM, CDGS; Writing − Review and Editing − ADS, CM, QZ, MEM, EAG, CDGS

Disclaimer

The content of this study is solely the responsibility of the authors and does not necessarily represent the official views of the NIH.

SUPPLEMENTARY MATERIAL

Supplementary material is linked to the online version of the paper at www.jidonline.org, and at https://doi.org/10.1016/j.jid.2022.12.009

REFERENCES

Bikle D, Christakos S. New aspects of vitamin D metabolism and action - addressing the skin as source and target. Nat Rev Endocrinol 2020;16: 234−52.

Bikle DD. Vitamin D metabolism and function in the skin. Mol Cell Endocrinol 2011;347:80−9.

Bikle DD, Elalieh H, Chang S, Xie Z, Sundberg JP. Development and progression of alopecia in the vitamin D receptor null mouse. J Cell Physiol 2006;207:340−53.

Carlberg C. Molecular basis of the selective activity of vitamin D analogues. J Cell Biochem 2003;88:274−81.

Chen J, Doroudi M, Cheung J, Grozier AL, Schwartz Z, Boyan BD. Plasma membrane Pdia3 and VDR interact to elicit rapid responses to 1alpha,25(OH)(2)D(3). Cell Signal 2013;25:2362−73.

de Guzman Strong C, Conan S, Deming CB, Cheng J, Sears KE, Segre JA. A milieu of regulatory elements in the epidermal differentiation complex syntenic block: implications for atopic dermatitis and psoriasis. Hum Mol Genet 2010;19:1453−60.

DeSantis TZ, Hugenholtz P, Larsen N, Rojas M, Brodie EL, Keller K, et al. Greengenes, a chimera-checked 16S rRNA gene database and workbench compatible with ARB. Appl Environ Microbiol 2006;72:5069−72.

Djian P, Easley K, Green H. Targeted ablation of the murine involucrin gene. J Cell Biol 2000;151:381−8.

Djian P, Green H. Vectorial expansion of the involucrin gene and the relatedness of the hominoids. Proc Natl Acad Sci USA 1989;86:8447−51.

Eckert RL, Green H. Structure and evolution of the human involucrin gene. Cell 1986;46:583−9.

Hahn JM, Supp DM. Abnormal expression of the vitamin D receptor in keloid scars. Burns 2017;43:1506−15.

Hao Y, Hao S, Andersen-Nissen E, Mauck WM 3rd, Zheng S, Butler A, et al. Integrated analysis of multimodal single-cell data. Cell 2021;184: 3573−87.e29.

Horiuchi N, Clemens TL, Schiller AL, Holick MF. Detection and developmental changes of the 1,25-(OH)2-D3 receptor concentration in mouse skin and intestine. J Invest Dermatol 1985;84:461−4.

Hosomi J, Hosoi J, Abe E, Suda T, Kuroki T. Regulation of terminal differentiation of cultured mouse epidermal cells by 1 alpha,25-dihydroxyvitamin D3. Endocrinology 1983;113:1950−7.

Hussain M, Borcard L, Walsh KP, Pena Rodriguez M, Mueller C, Kim BS, et al. Basophil-derived IL-4 promotes epicutaneous antigen sensitization concomitant with the development of food allergy. J Allergy Clin Immunol 2018;141:223−34.e5.

Igawa S, Di Nardo A. Skin microbiome and mast cells. Transl Res 2017;184: 68−76.

Jablonski NG, Chaplin G. Colloquium paper: human skin pigmentation as an adaptation to UV radiation. Proc Natl Acad Sci USA 2010;107(Suppl 2): 8962−8.

Joost S, Zeisel A, Jacob T, Sun X, La Manno G, Lönnerberg P, et al. Single-cell transcriptomics reveals that differentiation and spatial signatures shape epidermal and hair follicle heterogeneity. Cell Syst 2016;3: 221−37.e9.

Kajava AV. alpha-Helical solenoid model for the human involucrin. FEBS Lett 2000;473:127−31.

Kim BS, Siracusa MC, Saenz SA, Noti M, Monticelli LA, Sonnenberg GF, et al. TSLP elicits IL-33-independent innate lymphoid cell responses to promote skin inflammation. Sci Transl Med 2013;5:170ra16.

Kim BS, Wang K, Siracusa MC, Saenz SA, Brestoff JR, Monticelli LA, et al. Basophils promote innate lymphoid cell responses in inflamed skin. J Immunol 2014;193:3717−25.

Kobayashi T, Glatz M, Horiuchi K, Kawasaki H, Akiyama H, Kaplan DH, et al. Dysbiosis and Staphylococcus aureus colonization drives inflammation in atopic dermatitis. Immunity 2015;42:756−66.

Korsunsky I, Millard N, Fan J, Slowikowski K, Zhang F, Wei K, et al. Fast, sensitive and accurate integration of single-cell data with Harmony. Nat Methods 2019;16:1289−96.

Li M, Hener P, Zhang Z, Kato S, Metzger D, Chambon P. Topical vitamin D3 and low-calcemic analogs induce thymic stromal lymphopoietin in mouse keratinocytes and trigger an atopic dermatitis. Proc Natl Acad Sci USA 2006;103:11736−41.

Liberzon A, Birger C, Thorvaldsdóttir H, Ghandi M, Mesirov JP, Tamayo P. The Molecular Signatures Database (MSigDB) hallmark gene set collection. Cell Syst 2015;1:417−25.

Love MI, Huber W, Anders S. Moderated estimation of fold change and dispersion for RNA-seq data with DESeq2. Genome Biol 2014;15:550.

Makin G, Lohnes D, Byford V, Ray R, Jones G. Target cell metabolism of 1,25-dihydroxyvitamin D3 to calcitroic acid. Evidence for a pathway in kidney and bone involving 24-oxidation. Biochem J 1989;262:173−80.

Mathyer ME, Brettmann EA, Schmidt AD, Goodwin ZA, Oh IY, Quiggle AM, et al. Selective sweep for an enhancer involucrin allele identifies skin barrier adaptation out of Africa. Nat Commun 2021;12:2557.

Matsui T, Amagai M. Dissecting the formation, structure and barrier function of the stratum corneum [published correction appears in Int Immunol 2017;29:243−4] Int Immunol 2015;27:269−80.

McMurdie PJ, Holmes S. phyloseq: an R package for reproducible interactive analysis and graphics of microbiome census data. PLoS One 2013;8: e61217.

Meisel JS, Sfyroera G, Bartow-McKenney C, Gimblet C, Bugayev J, Horwinski J, et al. Commensal microbiota modulate gene expression in the skin. Microbiome 2018;6:20.

Mischke D, Korge BP, Marenholz I, Volz A, Ziegler A. Genes encoding structural proteins of epidermal cornification and S100 calcium-binding proteins form a gene complex ("epidermal differentiation complex") on human chromosome 1q21. J Invest Dermatol 1996;106:989−92.

Moosbrugger-Martinz V, Schmuth M, Dubrac S. A mouse model for atopic dermatitis using topical application of vitamin D3 or of its analog MC903. Methods Mol Biol 2017;1559:91−106.

Moskovicz V, Ben-El R, Horev G, Mizrahi B. Skin microbiota dynamics following B. subtilis formulation challenge: an in vivo study in mice. BMC Microbiol 2021;21:231.

Muehleisen B, Bikle DD, Aguilera C, Burton DW, Sen GL, Deftos LJ, et al. PTH/PTHrP and vitamin D control antimicrobial peptide expression and susceptibility to bacterial skin infection. Sci Transl Med 2012;4:135ra66.

Nemes Z, Marekov LN, Steinert PM. Involucrin cross-linking by transglutaminase 1. Binding to membranes directs residue specificity. J Biol Chem 1999;274:11013−21.

Niec RE, Rudensky AY, Fuchs E. Inflammatory adaptation in barrier tissues. Cell 2021;184:3361−75.

Oda Y, Uchida Y, Moradian S, Crumrine D, Elias PM, Bikle DD. Vitamin D receptor and coactivators SRC2 and 3 regulate epidermis-specific sphingolipid production and permeability barrier formation. J Invest Dermatol 2009;129:1367−78.

Ormerod KL, Wood DL, Lachner N, Gellatly SL, Daly JN, Parsons JD, et al. Genomic characterization of the uncultured Bacteroidales family S24-7 inhabiting the guts of homeothermic animals. Microbiome 2016;4:36.

Pillai S, Bikle DD, Elias PM. 1,25-Dihydroxyvitamin D production and receptor binding in human keratinocytes varies with differentiation. J Biol Chem 1988;263:5390−5.

Quack M, Carlberg C. The impact of functional vitamin D(3) receptor conformations on DNA-dependent vitamin D(3) signaling. Mol Pharmacol 2000;57:375−84.

Reddy GS, Tserng KY. Calcitroic acid, end product of renal metabolism of 1, 25-dihydroxyvitamin D3 through C-24 oxidation pathway. Biochemistry 1989;28:1763−9.

Ren D, Gong S, Shu J, Zhu J, Rong F, Zhang Z, et al. Mixed *Lactobacillus plantarum* strains inhibit *Staphylococcus aureus* induced inflammation and ameliorate intestinal microflora in mice. BioMed Res Int 2017;2017:7476467.

Rice RH, Green H. Presence in human epidermal cells of a soluble protein precursor of the cross-linked envelope: activation of the cross-linking by calcium ions. Cell 1979;18:681−94.

Robinson NA, LaCelle PT, Eckert RL. Involucrin is a covalently crosslinked constituent of highly purified epidermal corneocytes: evidence for a common pattern of involucrin crosslinking in vivo and in vitro. J Invest Dermatol 1996;107:101−7.

Roehr JT, Dieterich C, Reinnert K. Flexbar 3.0 - SIMD and multicore parallelization. Bioinformatics 2017;33:2941−2.

Romney ALT, Davis EM, Corona MM, Wagner JT, Podrabsky JE. Temperature-dependent vitamin D signaling regulates developmental trajectory associated with diapause in an annual killifish. Proc Natl Acad Sci USA 2018;115:12763−8.

Sanin DE, Ge Y, Marinkovic E, Kabat AM, Castoldi A, Caputa G, et al. A common framework of monocyte-derived macrophage activation. Sci Immunol 2022;7:eabl7482.

Schauber J, Dorschner RA, Coda AB, Büchau AS, Liu PT, Kiken D, et al. Injury enhances TLR2 function and antimicrobial peptide expression through a vitamin D-dependent mechanism. J Clin Invest 2007;117:803−11.

Schlingmann KP, Kaufmann M, Weber S, Irwin A, Goos C, John U, et al. Mutations in CYP24A1 and idiopathic infantile hypercalcemia. N Engl J Med 2011;365:410−21.

Sevilla LM, Nachat R, Groot KR, Klement JF, Uitto J, Djian P, et al. Mice deficient in involucrin, envoplakin, and periplakin have a defective epidermal barrier. J Cell Biol 2007;179:1599−612.

Steinert PM, Marekov LN. The proteins elafin, filaggrin, keratin intermediate filaments, loricrin, and small proline-rich proteins 1 and 2 are isodipeptide cross-linked components of the human epidermal cornified cell envelope. J Biol Chem 1995;270:17702−11.

Stumpf WE, Sar M, Reid FA, Tanaka Y, DeLuca HF. Target cells for 1,25-dihydroxyvitamin D3 in intestinal tract, stomach, kidney, skin, pituitary, and parathyroid. Science 1979;206:1188−90.

Subramanian A, Tamayo P, Mootha VK, Mukherjee S, Ebert BL, Gillette MA, et al. Gene set enrichment analysis: a knowledge-based approach for interpreting genome-wide expression profiles. Proc Natl Acad Sci USA 2005;102:15545−50.

Teumer J, Green H. Divergent evolution of part of the involucrin gene in the hominoids: unique intragenic duplications in the gorilla and human. Proc Natl Acad Sci USA 1989;86:1283−6.

Tseng H, Green H. The involucrin gene of the owl monkey: origin of the early region. Mol Biol Evol 1989;6:460−8.

Uberoi A, Bartow-McKenney C, Zheng Q, Flowers L, Campbell A, Knight SAB, et al. Commensal microbiota regulates skin barrier function and repair via signaling through the aryl hydrocarbon receptor. Cell Host Microbe 2021;29:1235−48.e8.

Villani AC, Satija R, Reynolds G, Sarkizova S, Shekhar K, Fletcher J, et al. Single-cell RNA-seq reveals new types of human blood dendritic cells, monocytes, and progenitors. Science 2017;356:eaah4573.

Volz A, Korge BP, Compton JG, Ziegler A, Steinert PM, Mischke D. Physical mapping of a functional cluster of epidermal differentiation genes on chromosome 1q21. Genomics 1993;18:92−9.

Walsh CM, Hill RZ, Schwendinger-Schreck J, Deguine J, Brock EC, Kucirek N, et al. Neutrophils promote CXCR3-dependent itch in the development of atopic dermatitis. ELife 2019;8:e48448.

Wang Z, Mascarenhas N, Eckmann L, Miyamoto Y, Sun X, Kawakami T, et al. Skin microbiome promotes mast cell maturation by triggering stem cell factor production in keratinocytes. J Allergy Clin Immunol 2017;139:1205−16.e6.

Watt FM. Mammalian skin cell biology: at the interface between laboratory and clinic. Science 2014;346:937−40.

Xie Z, Komuves L, Yu QC, Elalieh H, Ng DC, Leary C, et al. Lack of the vitamin D receptor is associated with reduced epidermal differentiation and hair follicle growth. J Invest Dermatol 2002;118:11−6.

Zhang C, Dowd DR, Staal A, Gu C, Lian JB, van Wijnen AJ, et al. Nuclear coactivator-62 kDa/Ski-interacting protein is a nuclear matrix-associated coactivator that may couple vitamin D receptor-mediated transcription and RNA splicing. J Biol Chem 2003;278:35325−36.

Zhao XP, Elder JT. Positional cloning of novel skin-specific genes from the human epidermal differentiation complex. Genomics 1997;45:250−8.

Zheng Q, Bartow-McKenney C, Meisel JS, Grice EA. HmmUFOtu: an HMM and phylogenetic placement based ultra-fast taxonomic assignment and OTU picking tool for microbiome amplicon sequencing studies. Genome Biol 2018;19:82.

Zheng Q, Grice EA. AlignerBoost: A generalized software toolkit for boosting next-gen sequencing mapping accuracy using a bayesian-based mapping quality framework. PLoS Comput Biol 2016;12:e1005096.

Zilionis R, Engblom C, Pfirschke C, Savova V, Zemmour D, Saatcioglu HD, et al. Single-cell transcriptomics of human and mouse lung cancers reveals conserved myeloid populations across individuals and species. Immunity 2019;50:1317−34.e10.

SUPPLEMENTARY MATERIALS AND METHODS

The following antibodies were used for flow cytometry: Fc block (CD16/CD32 [93, #14-0161-82], 1:400; eBioscience, San Diego, CA), CD4-phycoerythrin (PE) (Gk1.5, 1:400; BioLegend, San Diego, CA), CD8-allophycocyanin (APC) (53-6.7, 1:400; BioLegend), CD19-APC-Cy7 (1D3, 1:400; BD Pharmingen, San Jose, CA), CD11b-FITC (M1/70, 101205, 1:400; BioLegend), CD11c-PE-cyanin5 (N418, 1:400; eBioscience), Ly6g- PE-Cy7 (A8, 560601, 1:400; BD Biosciences, San Diego, CA), F4/80-PE (BM8, 12-4801-80, 1:400; Invitrogen, Waltham, MA), IgE-BV421 (R35-72, 564207, 1:200; BD Horizon, San Jose, CA), and CD45-APC (30-F11, 561018, 1:400; BD Pharmingen) (Cell Signaling Technology, 2021; Eberle et al., 2019). The following antibodies were used for flow cytometry isotype controls: FITC Rat IgG2b (A95-1, 556923, 1:400; BD Biosciences), PE-Cy7 Rat IgG2a (R35-95, 557855, 1:400; BD Biosciences), PE Rat IgG2a (R35-95, 551799, 1:400; BD Biosciences), APC-Cy7 Rat IgM (R4-22, 560571, 1:200; BD Biosciences), BV421 Rat IgG1 (R3-34, 562868, 1:200; BD Biosciences), and APC Rat IgG2b (A95-1, 553991, 1:400; BD Biosciences).
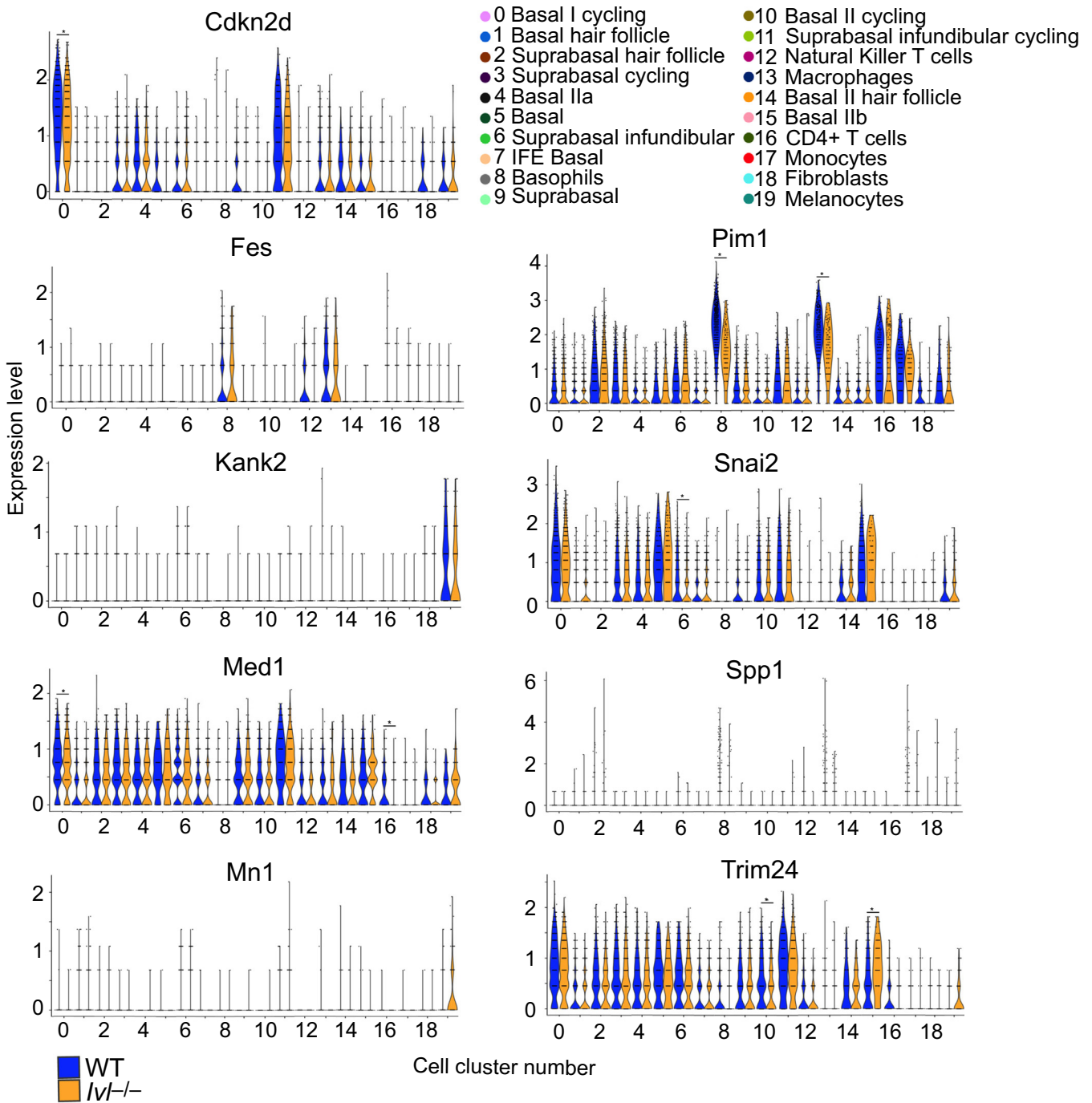
SUPPLEMENTARY REFERENCES

Cell Signaling Technology. Mouse immune cell marker guide. https://media.cellsignal.com/www/pdfs/science/pathways/Immune-Cell-Markers-Mouse.pdf; 2021. (accessed March 31, 2021).

JU Eberle, Radtke D, Nimmerjahn F, Voehringer D. Eosinophils mediate basophil-dependent allergic skin inflammation in mice. J Invest Dermatol 2019;139:1957−65.e2.
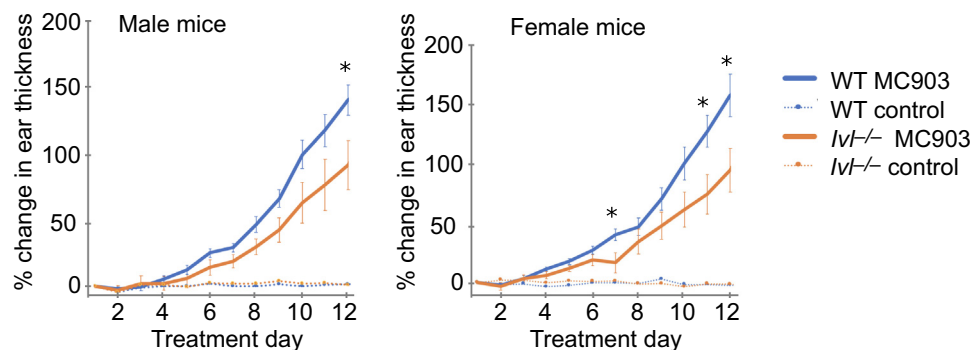
Supplementary Figure S1. *Ivl⁻/⁻* males and females exhibit trends similar to those of each other and for decreased MC903-treated skin inflammation compared with WT males and females. $Ivl^{-/-}$ males and females show relatively similar inflammatory responses and also decreased inflammation in comparison with WT males and females. Percentage change in ear thickness was significantly reduced in MC903-treated $Ivl^{-/-}$ males (n = 5) compared with that in treated WT males (n = 9) on day 12 and was also significantly reduced in MC903-treated $Ivl^{-/-}$ females (n = 5) compared with that in treated WT females (n = 6) on days 7, 11, and 12. *$P < 0.05$; one-way ANOVA with posthoc Tukey HSD. Data are presented as error bars ± SEM. HSD, honestly significant difference; IVL, involucrin; WT, wild-type.

Supplementary Figure S2. scRNA-seq identifies differential expressions for vitamin D−responsive genes in scRNA-seq cell clusters in MC903-treated *Ivl*⁻/⁻ versus in WT skin. IVL, involucrin; scRNA-seq, single-cell RNA sequencing; WT, wild type.

Supplementary Figure S3. *Ivl*$^{-/-}$ **mice exhibit similar MC903-treated immune infiltrate responses as WT mice.** No significant differences were found for dendritic cells (CD11c+), B cells (CD19+), neutrophils (CD11b+, Ly6g+), and eosinophils (CD11b+, Ly6g$^-$) in MC903-treated *Ivl*$^{-/-}$ mice (n = 5) compared with that in WT mice (n = 5) after 12 days of daily MC903 treatment (one-sided *t*-test). IVL, involucrin; WT, wild-type.